The Evolution of Galaxies on Cosmological Timescales
ASP Conference Series, Vol. 3×10^8, *1999*
J. E. Beckman, and T. J. Mahoney, eds.

Detecting Extrasolar Planets with the Keck Interferometer

Mark Swain

JPL/Caltech, 4800 Oak Grove Dr., Pasadena CA 91109

Rachel Akeson

IPAC/Caltech, MS 100-22, Pasadena CA 91125

Abstract. We discuss the development of the "Differential Phase" detection technique for the Keck Interferometer "Hot Jupiter" Key Science Program. The goal of the "Hot Jupiter" Key Science Program is the direct detection and infrared, low-resolution spectroscopic characterization of previously detected, T $\geq$ 1000 K extrasolar planets. Although many extrasolar planets are sufficiently bright to detect with large telescopes, the proximity of these planets to the much brighter stellar primary makes direct detection difficult because of angular resolution and intensity dynamic range limitations.

The Keck Interferometer, working in the near infrared, has sufficient angular resolution and sensitivity to detect some of the currently known extrasolar planets; however, the intensity dynamic range required (1:50,000) is substantially beyond the capability of the traditional techniques of optical and infrared direct-detection interferometers. The differential phase technique is a multi-wavelength, self-referenced phase measurement which relies on a chromatic, asymmetric brightness distribution to effectively convert a problem of intensity dynamic range into one of phase dynamic range. We report on the demonstration of this technique at the Palomar Testbed Interferometer and discuss the application of the technique to the Keck Interferometer.

1. Introduction

Direct detection of extrasolar planets is challenging due to the high intensity contrast and small angular separation between the planet and the star. For example, the planet/stellar thermal flux ratio of a Jupiter-size planet orbiting 0.05 pc from a solar-type star is $\sim 10^{-8}$ in the optical. In the infrared, this ratio becomes more tractable; the same system has a flux ratio of $\sim 10^{-4}$ at 2 μm. While the planet alone could be detected at this level, the nearby star makes this detection a problem of intensity dynamic range and spatial resolution. At a distance of 20 pc to the star-planet system, the angular separation of the planetary companion is 2.5 milliarcseconds, smaller than the diffraction limit of a single Keck 10-m telescope. Interferometric techniques can provide both the necessary sensitivity and resolution to study extrasolar planets in the infrared.

2. The Keck Interferometer

The Keck Interferometer project will connect the two 10-m Keck telescopes and add four 1.8-m outrigger telescopes for imaging and astrometry. This NASA-funded project has three Key Science areas:

- Detection of exo-zodiacal emission around nearby stars (technique = nulling).
- Direct characterization of warm, giant planets (technique = differential phase).
- Astrometric detection of Uranus-mass planets to 20 pc.

The Keck interferometer will also have synthesis imaging capability with 3 milliarcsecond resolution at 2 μm.

The first two Key Science observing modes, differential phase and nulling will begin in 2001. Astrometry with the outriggers and guest investigator observations will begin in 2003. For more information on the Keck Interferometer project see `http://huey.jpl.nasa.gov/keck/`.

3. How the Interferometer Works

In this section we schematically describe how an optical or infrared interferometer like the Keck Interferometer works. For more information on optical interferometry see the review by Shao & Colavita (1992).

The light is collected by two telescopes and a delay line is used to match the optical path length (Figure 1a). The light from each telescope is combined with a beam splitter and directed onto a detector. The detected fringe intensity can be modulated by moving the delay line away from the equal path length position (Figure 1b, top). The fringe intensity is high when the optical path difference between the two arms is an integer number of wavelengths and low at (n + 1/2) wavelengths. The outer envelope of the fringe intensity is set by the detector bandwidth.

The fringe amplitude and phase are measured by starting with the delay line on the center fringe (zero optical path difference) and stroking the delay line over an optical distance of one wavelength. The photons in each of four bins, labeled A, B, C, and D are counted and combined to form the fringe amplitude and phase (Figure 1b, bottom) (see Colavita 1999 for a more details on this technique). In an ideal instrument, the amplitude squared and phase are then given by

$$V^2 = \frac{\pi}{2} \frac{\langle (A-C)^2 + (B-D)^2 \rangle}{\langle A+B+C+D \rangle^2}$$

$$\phi = \tan^{-1} \frac{B-D}{A-C}.$$

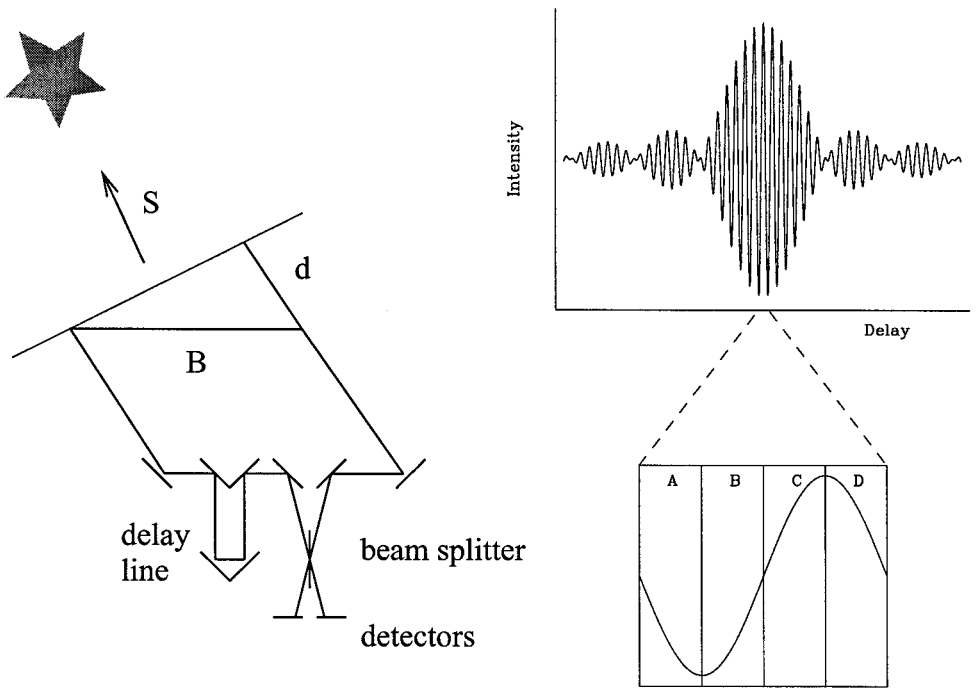

Figure 1. a) Left - A schematic of the interferometer. b) Right - The modulated intensity and fringe stroke.

4. Differential phase

In the differential phase mode, the presence of a faint companion is detected by measuring the fringe phase simultaneously at two or more wavelengths. A phase difference as a function of wavelength is produced by two effects:

1. The separation between the two sources as a fraction of a fringe depends on the wavelength.

2. For sources with different spectral energy distributions, the source fluxes will contribute different fractions of the total received intensity at different wavelengths, producing a phase difference (Figure 2).

This effect can be quantitatively derived as follows. In the narrow band limit, the fringe from the primary is given by

$$V_p \cos(kx)$$

where k is $2\pi/\lambda$ and x is the delay. The secondary source fringe is given by

$$V_s \cos[k(x+\delta)],$$

where δ is the separation of the two sources on the sky as measured in delay space and is a function of the baseline and ds, the separation on the sky, $\delta = \vec{ds} \cdot \vec{B}$ (Figure 2). Both the amplitudes of the fringes V_p and V_s, as well as k will depend on the wavelength band. The relative contribution of the primary and secondary to the photon count for a particular measurement bin, A, B, C, D, is given by

$$A_{\lambda_1} = \int_0^{\lambda_1/4} V_p \cos[k_1 x]\, dx + \int_0^{\lambda_1/4} V_s \cos[k_1 (x + \delta)]\, dx$$

and so on. Once the source flux densities and separation vector are specified, the phase at each wavelength and the differential phase can be easily computed from these integrals.

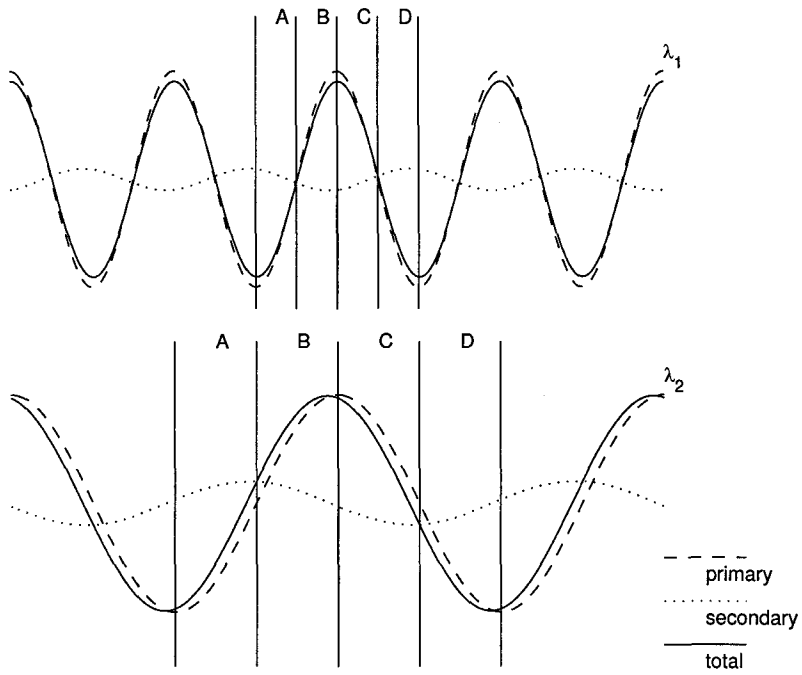

Figure 2. The fringes in delay space for the primary and secondary sources at different wavelengths. The wavelength difference and secondary/primary flux ratio have been exaggerated to show the differential phase. Note that the position of the central peak of the total fringe (solid line) has shifted - this is the differential phase.

As the interferometer tracks a source across the sky, the projected baseline will evolve in time. Thus, the differential phase for a given source will be a function of hour angle. This evolution of the differential phase can be used to distinguish the true signal from instrumental effects.

5. Observational Technique

As the maximum differential phase effect is approximately the relative source fluxes, it is essential to make very precise phase measurements. The phase sensitivity goal for the differential phase mode at the Keck Interferometer is 0.1 milliradians, although higher sensitivity may be possible with long integration times and with very closely spaced wavelengths. One of the two wavelengths will be used as the reference for fringe tracking. The phase at the second wavelength will be measured simultaneously as an offset phase from the reference wavelength. By using the same beam path for the 2 wavelengths and measuring the phases simultaneously, many systematic effects will be removed from the observed phase. Differential phase observations with the Keck Interferometer will be possible from H to M bands (1.6 to 5 μm) with currently planned instrumentation and possibly in the N band (10 μm).

One complication for these multi-wavelength observations is the wavelength dependence of the atmospheric dispersion. If this effect is not corrected, the fringe packets at the two wavelengths will not be at the same location in delay space. At the Keck Interferometer an atmospheric dispersion compensator (ADC) will be inserted into the optics path to equalize the phase delay at the two wavelengths. As part of the differential phase mode development, an ADC will be installed at the Palomar Testbed Interferometer. Test observations will be made between the H and K bands on known binary sources.

6. Extrasolar Giant Planets

The companions to nearby stars discovered through radial velocity searches are the best candidates for warm, Jupiter mass planets. As warmer planets will have a higher flux relative to the stellar flux, and therefore a larger differential phase, the planets with orbits smaller than 0.3 AU (Table 1) are the best targets for the Keck Interferometer.

Star Name	M*sini*	Period	Semi-major axis		Eccentricity
	M_J	days	AU	mas	
HD 187123	0.52	3.1	0.042	0.9	0.00
τ Bootis	3.64	3.3	0.042	2.7	0.00
51 Pegasi	0.44	4.2	0.051	3.3	0.01
υ Andromedae	0.63	4.6	0.053	3.9	0.03
HD 217107	1.28	7.1	0.07	3.5	0.14
ρ^1 55 Cancri	0.85	14.6	0.12	9.6	0.03
Gliese 86	3.6	15.8	0.11	10.1	0.04
HD 195019	3.43	18.3	0.14	3.7	0.05
ρ Corona Borealis	1.1	39.6	0.23	13.2	0.1

Table 1. Masses and orbital characteristics of some candidate extrasolar planet systems. This list is taken from G. Marcy's web page.

Observations utilizing radial velocity variations of stellar spectral lines to search for planetary companions yield the companion mass times the sine of the inclination and the orbit. Predictions for the composition and temperature of these planets come from modeling, extrapolation from our own solar system and recent spectral data from cool brown dwarfs such as Gliese 229B.

If the planet emits as a blackbody (see discussion below), the flux is determined by the planet's effective temperature and radius. In models for brown dwarfs and giant planets, the radius is roughly independent of mass and is $\sim 8 \times 10^9$ cm (1.1 R_J) for planets older than 10^8 years (Saumon et al. 1996; Burrows et al. 1997). The effective temperature of each planet listed above can be calculated given the stellar spectral type and an estimate of the albedo (Table 2).

Star Name	Spectral type	T_* K	T_{planet} K
HD 187123	G5	5770	1180
τ Bootis	F6	6360	1660
51 Pegasi	G2	5850	1200
υ Andromedae	F8	6200	1500
HD 217107	G8	5570	880
ρ^1 55 Cancri	G8	5570	630
Gliese 86	K1	5080	600
HD 195019	G3	5830	690
ρ Corona Borealis	G0	6030	460

Table 2. Spectral characteristics of central stars. The planet effective temperature is given for an albedo of 0.3. Spectral types are from SIMBAD and the effective temperatures are from Gonzalez (1998).

To investigate the range of differential phase signatures possible from the close-in systems, we have examined models from Allard (1999), Goukenleuque et al. (1999) and Seager, Whitney & Sasselov (1999). Models of isolated planets and brown dwarfs such as Allard et al. (1996) and Burrows et al. (1997) are not applicable for the close-in planets due to the intense stellar radiation. A close-in planet will have a different atmospheric temperature-pressure profile as compared to an isolated planet with the same effective temperature. At the small star-planet separations considered here, reflected light from the primary will be important in some spectral regions. The models of both Goukenleuque et al. (1999) and Seager & Sasselov (1998) show that while reflected light will dominate thermal emission in the planet's spectrum at optical wavelengths, the reflected component is not substantial at near-infrared and longer wavelengths.

All three groups mentioned above have produced models for 51 Peg, and these are the models we have used in estimating the differential phase effect. Although all groups find effective temperatures in the range 1200-1300 K, the predicted infrared spectra vary from a nearly featureless, almost blackbody spectrum (Allard) to strong departures from blackbody due to molecular lines (Seager and Goukenleuque). An example spectra from Goukenleuque et al. (1999)

is shown in Figure 3. Estimates of the differential phase effect for each model between the relevant infrared bands is given in Table 3.

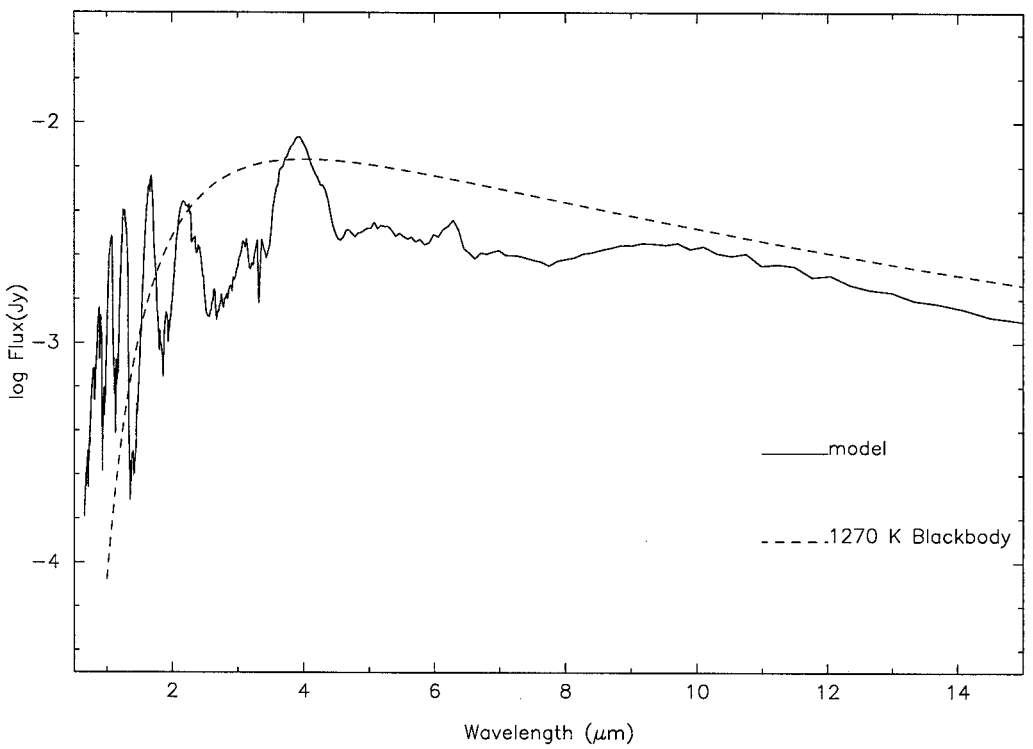

Figure 3. A model spectrum (solid line) for the planet orbiting 51 Peg from Goukenleuque et al. (1999) and a blackbody spectrum at Teff = 1270 (dashed line).

Model	H–K	K–L	L–M	8.75–11μm
51 Peg				
Goukenleuque	0.06	0.15	0.12	0.06
Allard (1270 K blackbody)	0.07	0.27	0.27	0.04
Seager	0.10	0.32	0.30	0.10

Table 3. Predicted differential phase in milliradians between the near-infrared bands for various models of 51 Peg.

By modeling the data obtained from differential phase observations, the flux as a function of wavelength can be derived. This can be used to estimate the following properties of the extrasolar giant planets:

Effective temperature Estimate using the flux in line-free regions of the spectrum and models for the planetary radius.

Spectral features The Keck Interferometer will have a spectral resolution of $\sim$100. Departures from a blackbody spectrum, particularly in the near-infrared could indicate the presence of molecules such as methane.

Orbital parameters Measuring the differential phase throughout an orbital period will yield the inclination, and thus the true planetary mass.

7. Other targets

The NASA Key Science program will use differential phase to study warm, Jupiter mass planets. There are many other kinds of astronomical sources which can benefit from an observational method which allows study of faint emission near a bright source. This list includes:

- Spectroscopic single-line binaries.
- Brown dwarf binary companions.
- Asymmetries in circumstellar dust shells.

Acknowledgments. The research described in this paper was carried out by the Jet Propulsion Laboratory, California Institute of Technology, under a contract with the National Aeronautics and Space Administration.

References

Allard, F., 1999, this proceedings

Allard, F., Hauschildt, P.H., Baraffe, I., Chabrier, G., 1996, ApJ, 465, 123

Burrows, A., Marley, M., Hubbard, W.B., Lunine, J.L., Guillot, T., Saumon, D., Freedman, R., Sudarsky, D. & Sharp, C., 1997, ApJ, 491, 856

Colavita, M.M., 1999, PASP, 111, 111

Gonzalez, G., 1998, A&A, 334, 221

Goukenleuque, C., Bezard, B., Lellouch & Freedman, 1999, Icarus, in press

Saumon, D., Hubbard, W.B., Burrows, A., Guillot, T., Lunine, J.L. & Chabrier, G., 1996, ApJ, 460, 993

Seager, S. & Sasselov, D., 1998, ApJ, 502, L157

Seager, S., Whitney, B.A., & Sasselov, D.D. 1999, ApJ, submitted

Shao, M. & Colavita, M.M., 1992, ARA&A, 30, 457